frontiers | Frontiers in Environmental Science

TYPE Original Research
PUBLISHED 05 September 2025
DOI 10.3389/fenvs.2025.1622134

OPEN ACCESS

EDITED BY
Xiaofei Tan,
Hunan University, China

REVIEWED BY
Siroos Shojaei,
University of Sistan and Baluchestan, Iran
Halil Ibrahim Burgan,
Akdeniz University, Türkiye

*CORRESPONDENCE
Vicky Jain,
vicky.jain@marwadieducation.edu.in

RECEIVED 02 May 2025
ACCEPTED 30 July 2025
PUBLISHED 05 September 2025

CITATION
Ahmad I, Alhedrawie D, Jain V, Kumar A, Rekha MM, Kundlas M, Sunitha S, Ray S and Shomurotova S (2025) Application of central composite design for optimizing and statistical analysis of ultrasound-assisted removal of dyes from aqueous solution.
Front. Environ. Sci. 13:1622134.
doi: 10.3389/fenvs.2025.1622134

Application of central composite design for optimizing and statistical analysis of ultrasound-assisted removal of dyes from aqueous solution

Irfan Ahmad[1], Dilshad Alhedrawie[2,3,4], Vicky Jain[5]*, Abhinav Kumar[6,7], M. M. Rekha[8], Mayank Kundlas[9], S. Sunitha[10], Subhashree Ray[11] and Shirin Shomurotova[12]

[1]Department of Clinical Laboratory Sciences, College of Applied Medical Sciences, King Khalid University, Abha, Saudi Arabia, [2]Department of Computer Techniques Engineering, College of Technical Engineering, The Islamic University, Najaf, Iraq, [3]Department of Computer Techniques Engineering, College of Technical Engineering, The Islamic University of Al Diwaniyah, Al Diwaniyah, Iraq, [4]Department of Computer Techniques Engineering, College of Technical Engineering, The Islamic University of Babylon, Babylon, Iraq, [5]Marwadi University Research Center, Department of Chemistry, Faculty of Science, Marwadi University, Rajkot, Gujarat, India, [6]Department of Nuclear and Renewable Energy, Ural Federal University Named after the First President of Russia Boris Yeltsin, Ekaterinburg, Russia, [7]Department of Mechanical Engineering, Karpagam Academy of Higher Education, Coimbatore, India, [8]Department of Chemistry and Biochemistry, School of Sciences, Jain (Deemed to be University), Bangalore, Karnataka, India, [9]Centre for Research Impact and Outcome, Chitkara University Institute of Engineering and Technology, Chitkara University, Rajpura, Punjab, India, [10]Department of Chemistry, Sathyabama Institute of Science and Technology, Chennai, Tamil Nadu, India, [11]Department of Biochemistry, IMS and SUM Hospital, Siksha 'O' Anusandhan (Deemed to be University), Bhubaneswar, Odisha, India, [12]Department of Chemistry Teaching Methods, Tashkent State Pedagogical University named after Nizami, Tashkent, Uzbekistan

Introduction: This research evaluates the potential of nickel ferrite magnetic nanoparticles (NFO) for the ultrasound-assisted removal of rhodamine B (RB) and safranin O (SO) from aqueous media. A central composite design (CCD) within the framework of response surface methodology (RSM) was employed to model, optimize, and analyze the removal process.

Methods: Meanwhile, the effects of solution pH (3-11), pollutant concentration (10–50 mg L^{-1}), NFO amount (0.01–0.03 g), and sonication time (10-50 min) were investigated systematically.

Results: Under optimized conditions determined by CCD (i.e., pH of 8, pollutant concentration of 20 mg L^{-1}, NFO amount of 0.038 g, and sonication time of 16 min), the removal efficiencies for RB and SO were achieved at 95.87% and 92.64%, respectively. The adsorbent characterization using scanning electron microscopy (SEM), energy-dispersive X-ray (EDX), Fourier-transform infrared (FTIR), X-ray diffraction (XRD), vibrating sample magnetometer (VSM), and point of zero charge (pH_{pzc}) analysis confirmed the nanometric particle size, high surface area, superparamagnetic properties, and a pH_{pzc} of 6.3 for NFO. Eluent studies indicated that ethanol provided the highest desorption efficiency, enabling effective regeneration of NFO nanoparticles over multiple cycles without significant loss of performance. Application to real water samples demonstrated the practical applicability of NFO, achieving high removal efficiencies while maintaining structural integrity and magnetic separability.

Discussion: These findings highlight the importance of NFO as a promising, reusable, and efficient adsorbent for the rapid removal of toxic dyes under ultrasonic assistance, contributing to the advancement of sustainable water treatment technologies.

KEYWORDS

central composite design, dyes, magnetic nanoparticles, nickel ferrite, ultrasound-assisted removal

1 Introduction

Water pollution caused by synthetic dyes has emerged as a critical environmental concern due to the extensive use of dyes in the textile, leather, and paper industries, as well as their persistence and toxicity in aquatic environments (Aragaw and Bogale, 2021; Tkaczyk et al., 2020). Among these dyes, RB and SO are widely used due to their bright colors and stability; however, their discharge into water bodies leads to serious ecological and health issues. The presence of these dyes in water can inhibit light penetration, disrupt photosynthetic activity, and have a negative impact on aquatic ecosystems (Jassim et al., 2025; Khandelwal et al., 2024). Additionally, many dyes exhibit carcinogenic and mutagenic properties, emphasizing the urgent need for effective treatment methods to remove them from wastewater before environmental discharge (Bopape et al., 2024; Shojaei et al., 2021).

Conventional treatment methods, including coagulation, membrane filtration, and advanced oxidation processes, have been applied for dye removal but often suffer from high operational costs, complex operation, and incomplete removal, particularly at low pollutant concentrations (Liu et al., 2025; Teweldebrihan et al., 2024; Alharbi et al., 2022; Peramune t al. 2022; Hoong and Ismail, 2018). Adsorption has gained significant attention as a promising approach for water and wastewater treatment owing to its simplicity, high efficiency, cost-effectiveness, and minimal production of secondary waste (Garg et al., 2025; Al-Saeedi et al., 2023). Choosing an efficient adsorbent with a high surface area and reusability plays a pivotal role in achieving effective dye removal.

In recent years, nanostructured materials have demonstrated remarkable potential as adsorbents regarding their high surface-to-volume ratio, tunable surface chemistry, and enhanced interaction with pollutants (Prabhu et al., 2023; Iqbal et al., 2022). However, the separation of nanoparticles from treated water can be challenging, limiting their practical application (Li et al., 2023). Magnetic nanoparticles, such as NFO, have emerged as attractive adsorbents considering their superparamagnetic properties, enabling easy recovery from aqueous solutions using an external magnetic field, thereby preventing secondary pollution and allowing repeated use (Singh et al., 2023). Moreover, NFO nanoparticles possess a high surface area and stability under various environmental conditions, making them suitable candidates for dye removal applications (Hassan et al., 2025).

Ultrasound-assisted removal has gained increasing attention in water treatment because of its ability to enhance mass transfer, reduce equilibrium time, and improve pollutant removal efficiency. The application of ultrasonic waves generates acoustic cavitation, leading to the formation and collapse of microbubbles in the solution, which creates localized high temperatures and pressures (Kalsoom et al., 2024). These micro-environments promote the breakdown of dye aggregates and improve the dispersion of adsorbent particles, thereby increasing the availability of active sites for pollutant removal (Çalışkan and Şayan, 2024). Additionally, ultrasonication can facilitate the desorption of pollutants from the adsorbent surface during regeneration cycles, further enhancing the reusability of the adsorbent material (Bayuo et al., 2024). Considering these advantages, the integration of ultrasonication with adsorption processes has emerged as an effective strategy for the rapid and efficient removal of dyes from aqueous media.

Optimization of operating parameters is essential to maximize process efficiency and understand the interaction effects of process variables (Ugural et al., 2024). RSM serves as a robust statistical tool to design experiments systematically, evaluate the influence of multiple factors, and identify optimal conditions with a reduced number of experiments (He et al., 2023). CCD, as a widely used approach within RSM, facilitates the development of predictive models and the analysis of variable interactions, thereby enhancing the efficiency of removal studies (Oza et al., 2022; Yang et al., 2022).

For instance, Sarkar et al. employed RSM to model and optimize the removal of safranin using nano-silica-coated peanut shell-derived biochar composite. By investigating the interactive effects of variables such as pH, adsorbent dosage, and dye concentration, they successfully achieved over 97.22% removal efficiency for safranin. The optimal conditions determined through RSM were pH of 8, adsorbent dosage of 2 g, and dye concentration of 10 mg L^{-1} (Sarkar et al., 2025).

In another study, Hsu et al. applied RSM to optimize the removal of crystal violet (CV), tetracycline (TC), and methylene blue (MB) using Fe_3O_4/rGO/Ag nanocomposite. Their results revealed maximum removal of 95.82% for CV, 91.33% for TC, and 98.19% for MB. The optimized conditions for maximum removal were obtained at a pH of 6, a time of 8 min, a nanocomposite amount of 0.014 g, and a concentration of 21 mg L^{-1} (Hsu et al., 2024).

Moreover, Ali et al. utilized RSM to investigate the removal of auramine O (AO) using sodium dodecylsulfate (SDS)–modified activated carbon (PA-AC-SDS) as the adsorbent. The optimal conditions for the removal process were determined as pH of 6, adsorbent dosage of 0.11 g, contact time of 240 min, and concentration of 1,000 mg L^{-1}. The maximum adsorption capacity was reported as 425.06 mg g^{-1} for AO (Ali et al., 2021).

In this research, NFO magnetic nanoparticles were synthesized and used for the ultrasound-assisted removal of RB and SO from aqueous media. The adsorbent was characterized using various analytical techniques to confirm its structure and surface properties. A CCD within the RSM framework was employed to optimize the removal process by evaluating the effects of pH,

TABLE 1 Chemical properties of RB and SO.

Analyte	Molecular formula	Molecular weight	λ_{max}	Structure
Rhodamine B (RB)	$C_{28}H_{31}ClN_2O_3$	479.02 g mol^{-1}	556 nm	
Safranin O (SO)	$C_{20}H_{19}ClN_4$	350.85 g mol^{-1}	525 nm	

pollutant concentration, adsorbent amount, and sonication time. Additionally, the reusability of NFO nanoparticles and their performance in real water samples were assessed to demonstrate their practical applicability in sustainable wastewater treatment.

2 Experimental

2.1 Materials and instrumentation

All chemicals used in this study were of analytical grade and used without further purification. Sodium hydroxide (NaOH), ferric chloride hexahydrate ($FeCl_3{\cdot}6H_2O$), acetonitrile (C_2H_3N), nickel chloride hexahydrate ($NiCl_2{\cdot}6H_2O$), formic acid (CH_2O_2), hydrochloric acid (HCl), ethanol (C_2H_6O), and toluene (C_7H_8) were purchased from Merck (Germany). Stock solutions of RB and SO (1,000 mg L^{-1}) were prepared in deionized water and diluted as required. The pH of the solutions was adjusted using 0.1 M NaOH and 0.1 M HCl solutions. All experiments were performed using deionized water. The surface morphology and particle size of NFO nanoparticles were characterized using SEM (TESCAN MIRA3). Structural analysis was performed using XRD (Philips PW 1800) with Cu Kα radiation. FTIR (Bruker Tensor 27) was used to analyze the surface functional groups of the nanoparticles. Magnetic properties were assessed using a VSM (BHV-55). The pH of solutions was measured with a pH meter (Metrohm 827). An ultrasonic device (Hielscher UP400S, 400 W, 24 kHz) was utilized for sonication during removal experiments. UV-Vis spectrophotometry (Shimadzu UV-1800) was employed to measure dye concentrations. The characteristics of RB and SO are presented in Table 1.

2.2 Synthesis of NFO nanoparticles

NFO nanoparticles were synthesized via a co-precipitation method under a nitrogen atmosphere to prevent the oxidation of Fe^{2+} ions during the synthesis. Initially, 2.38 g of $FeCl_3{\cdot}6H_2O$ and 0.95 g of $NiCl_2{\cdot}6H_2O$ were accurately weighed and dissolved in 100 mL of deoxygenated deionized water in a 250 mL three-neck flask under continuous nitrogen purging. The solution was magnetically stirred at 80°C to ensure complete dissolution and homogenization of the precursor salts. Subsequently, 20 mL of NaOH (2 M) solution was added dropwise to the reaction mixture under constant stirring at 80 °C, maintaining a pH around 11. The gradual addition of NaOH led to the formation of a black precipitate, indicating the formation of NFO nanoparticles. The reaction mixture was maintained at 80 °C under constant stirring for an additional 2 h to allow for complete precipitation and crystallization of the nanoparticles. After the reaction was completed, the black precipitate was separated from the reaction medium using a strong neodymium magnet and washed several times with deionized water to remove unreacted ions, followed by washing with ethanol to eliminate any remaining organic impurities. The washed precipitate was then oven-dried at 70 °C for 12 h. To improve the crystallinity of the synthesized NFO nanoparticles, the dried powder was calcined in a muffle furnace at 500 °C for 3 h under an air atmosphere. As a result, highly crystalline NFO nanoparticles suitable for further characterization and adsorption experiments were produced (Hariharasuthan et al., 2022). The synthesis procedure of NFO nanoparticles is illustrated in Figure 1.

2.3 Determination of pH_{pzc}

The pH_{pzc} is defined as the pH at which the surface of the adsorbent carries a net zero charge. This parameter plays a crucial role in controlling the electrostatic interactions between the adsorbent surface and charged dye molecules during the adsorption process. In this study, the pH_{pzc} of NFO was determined using the pH drift method. For this purpose, 50 mL of 0.01 M NaCl solution was adjusted to different initial pH values ranging from two to 9 using 0.1 M HCl or 0.1 M NaOH. Then, 0.05 g of NFO nanoparticles was added to each solution, and the suspensions were stirred for 48 h at room temperature. The final pH was measured, and the pH_{pzc} was determined from the plot of ΔpH (pH_{final} - $pH_{initial}$) versus $pH_{initial}$ where ΔpH equals zero.

2.4 Experimental design using RSM

RSM is a widely applied statistical and mathematical tool for modeling and optimizing complex processes with multiple variables. This technique enables the evaluation of both individual and interactive effects of factors on the response, while minimizing the number of experiments. In this study, a CCD, one of the most effective designs within RSM, was employed to optimize the conditions for the ultrasound-assisted removal of RB and SO using NFO nanoparticles as the adsorbent. Four independent variables were selected for optimization, including the amount of NFO nanoparticles (0.01–0.05 g), the pH of the solution (3–11), the pollutant concentration (10–50 mg L^{-1}), and the sonication time (5–25 min). Each of these variables was studied at five coded levels (−2, −1, 0, +1, and +2), systematically covering the experimental domain to capture the influence of each parameter on the removal efficiency (Table 2).

In the CCD applied in this study, the total number of experimental runs was determined using Equation 1.

$$N = 2^k + 2k + n_c \quad (1)$$

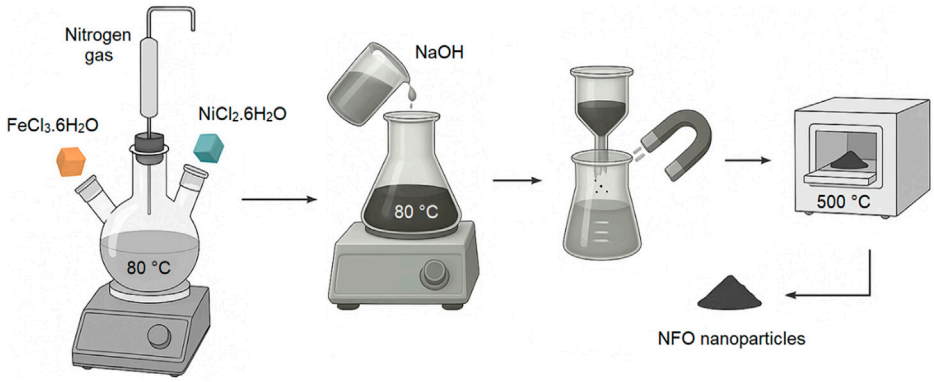

FIGURE 1
Schematic illustration of the synthesis procedure of NFO nanoparticles.

TABLE 2 The design of CCD.

Variables	Symbol	Unit	Levels					Step change value
			−2	−1	0	+1	+2	
NFO amount	A	g	0.01	0.02	0.03	0.04	0.05	0.01
pH of the solution	B	—	3	5	7	9	11	2
Pollutant concentration	C	mg L^{-1}	10	20	30	40	50	10
Sonication time	D	min	5	10	15	20	25	5

where k represents the number of independent variables and n_c is the number of replicates at the center points to estimate the pure error and verify the reproducibility of the experiments. Considering four independent variables in this research (i.e., pH, pollutant concentration, NFO amount, and sonication time), the total number of experiments calculated was 30 runs. The 30 experiments included 16 factorial points, 8 axial points, and 6 center points to ensure model reliability and accurate estimation of experimental error (Table 3). The experimental data were fitted to a second-order polynomial model expressed in Equation 2.

$$Y = \beta_0 + \sum_{i=1}^{k}\beta_i X_i + \sum_{i=1}^{k}\beta_{ii} X_i^2 + \sum_{i\le j}^{k}\sum_{j}^{k}\beta ij X_i X_j \quad (2)$$

where Y represents the predicted response (removal of dye), β_0 is the intercept term, β_i denotes the linear coefficients, β_{ii} is the quadratic coefficients, β_{ij} shows the interaction coefficients, and X_i and X_j are the coded independent variables.

Design Expert software (Version 12, Stat-Ease Inc., USA) was used to design the experimental runs, analyze the results, and generate three-dimensional response surface and contour plots to visualize the effects of variables and their interactions on dye removal efficiency. The adequacy of the developed models was assessed based on the coefficient of determination (R^2), adjusted R^2, and predicted R^2, where values closer to 1 indicated a better fit of the model to the experimental data. The significance of the model and its terms was evaluated using analysis of variance (ANOVA) at a 95% confidence level ($p < 0.05$). Furthermore, the mean square error (MSE) and root mean square error (RMSE) were calculated using Equations 3, 4 to evaluate the predictive performance and accuracy of the developed quadratic models.

$$MSE = \frac{1}{n}\sum_{i=1}^{n}\left(y_i{}^{exp} - y_i^{pred}\right)^2 \quad (3)$$

$$RMSE = \sqrt{\frac{1}{n}\sum_{i=1}^{n}\left(y_i{}^{exp} - y_i^{pred}\right)^2} \quad (4)$$

where $y_i{}^{exp}$ and y_i^{pred} represent the experimental and predicted values, respectively, and n is the total number of experimental runs. Lower values of MSE and RMSE reflect higher model accuracy and indicate the developed models' robustness in predicting dye removal efficiencies under various operational conditions.

Numerical optimization was performed using the desirability function within the software to identify the optimal conditions for simultaneously maximizing the removal of RB and SO, assigning equal importance to both responses. The desirability value, which ranges from 0 to 1, was used to determine the conditions under which the highest removal efficiencies could be achieved.

2.5 Ultrasound-assisted removal experiments

Adsorption experiments were performed in 100 mL glass beakers containing 50 mL of dye solutions at predetermined

concentrations and pH levels (Table 2). A certain amount of NFO nanoparticles was added to the solution, and the mixture was subjected to ultrasonication under continuous stirring for the specified sonication time. After sonication, the NFO nanoparticles were separated from the solution using an external magnet. Besides, the supernatant was analyzed using a UV-Vis spectrophotometer at the maximum absorption wavelengths of RB and SO. The removal efficiency (R%) was calculated using Equation 5.

$$\%Removal = \frac{C_0 - C_f}{C_0} \times 100 \quad (5)$$

where C_0 (mg L^{-1}) and C_f (mg L^{-1}) represent the initial and final concentrations of the dyes, respectively.

3 Results and discussion

3.1 Characterization of NFO nanoparticles

The synthesized NFO nanoparticles were characterized using SEM, XRD, FTIR, EDX, VSM, and pHpzc analyses to confirm their morphology, crystallinity, surface functional groups, magnetic properties, and surface charge behavior. XRD analysis was performed to analyze and determine the crystal structure of NFO nanoparticles, as shown in Supplementary Figure S1a. XRD patterns confirmed the formation of crystalline NFO, displaying characteristic peaks at 2θ values of 30.73°, 35.29°, 36.93°, 43.96°, 53.61°, 57.42°, and 62.91°, corresponding to the (220), (311), (222), (400), (422), (511), and (440) planes, respectively. These angles are in agreement with the standard magnetite pattern (JCPDS No. 10–0325) (Sivakumar et al., 2013). Using the Debye–Scherrer equation, the average crystallite size was estimated to be around 40 nm. According to SEM image (Supplementary Figure S1b), the NFO nanoparticles revealed a near-spherical morphology with uniform distribution and an average particle size of approximately 70 nm, indicating their suitability for adsorption applications owing to their high surface area and homogeneity. FT-IR spectroscopy was used to identify the functional groups. In the FT-IR spectrum of NFO nanoparticles shown in Supplementary Figure S1c, the peaks at 608 cm^{-1} and 456 cm^{-1} are related to the stretching vibration of Fe-O and Ni-O, respectively. Additionally, bands observed at 3,400 cm^{-1} and 1,630 cm^{-1} were associated with O-H stretching and bending vibrations, indicating the presence of surface hydroxyl groups. These groups can contribute to the adsorption of dye molecules through hydrogen bonding and electrostatic interactions. The results confirm the synthesis of NFO nanoparticles. VSM analysis was performed to measure the magnetic properties of the synthesized NFO nanoparticles (Supplementary Figure S1d). According to this analysis, the NFO nanoparticles exhibited superparamagnetic behavior with a saturation magnetization of 41.9 emu g^{-1}. As a result, they enabled the easy separation of nanoparticles from aqueous media using an external magnetic field, with minimal residual magnetization, thereby facilitating reuse. EDX was used to analyze the elemental composition of NFO nanoparticles. Supplementary Figure S1e shows the EDX spectrum of NFO nanoparticles. The presence of Fe, O, and Ni elements in the EDX spectrum suggests the proper synthesis of NFO nanoparticles. The pH_{pzc} of NFO was determined to be 6.3, indicating that the surface of NFO is positively charged at pH values below 6.3 and negatively charged at pH values above this value, which is critical in controlling the electrostatic interactions during dye removal (Supplementary Figure S1f).

3.2 Statistical analysis and model fitting

The CCD experimental data were analyzed using Design Expert software to evaluate the effects of pH, pollutant concentration, NFO amount, and sonication time on the removal efficiency of RB and SO. The ANOVA results demonstrated that the developed quadratic models were significant for both RB and SO removal, with p-values less than 0.0001 (Supplementary Tables S1, S2). Therefore, there is a strong correlation between the experimental and predicted data. The R^2 values for the RB and SO removal models were found to be 0.9997 and 0.9986, respectively. These values indicate that over 99% of the variability in the removal efficiency could be explained by the models. Additionally, the adjusted R^2 and predicted R^2 values were in close agreement, confirming the models' reliability and predictive capability. The lack of fit for both models was non-significant ($p > 0.05$), further indicating the adequacy of the models.

In this study, the MSE and RMSE were calculated to assess the predictive performance of the models further. For the RB removal model, the MSE and RMSE values were found to be 0.08 and 0.28, respectively. Meanwhile, for the SO removal model, the MSE and RMSE values were 0.40 and 0.63, respectively. These low values of MSE and RMSE indicate a high degree of accuracy in predicting dye removal efficiencies, confirming the models' capability for reliable estimation within the studied experimental domain. The developed models can be expressed in terms of coded variables, as shown in Equations 6, 7.

$$Y_{RB} = +84.89 + 8.36A + 6.39B - 10.18C + 5.79D + 1.60AB + 1.34AC + 1.58AD - 0.01BC + 0.21BD + 1.53CD - 6.04A^2 - 8.45B^2 - 5.60C^2 - 5.63D^2 \quad (6)$$

$$Y_{SO} = +90.41 + 6.94A + 7.95B - 9.01C + 4.19D + 0.94AB - 0.46AC + 1.04AD + 0.91BC - 0.67BD + 0.541CD - 6.87A^2 - 7.58B^2 - 5.76C^2 - 5.50D^2 \quad (7)$$

where Y_{RB} and Y_{SO} represent the removal percentages of RB and SO, respectively, while A, B, C, and D correspond to the coded values for NFO amount, pH, pollutant concentration, and sonication time, respectively.

To visually assess the predictive capability and residual behavior of the developed models, graphical analyses were conducted. Supplementary Figures S2a, b illustrate the plots of predicted values versus actual experimental values for the removal efficiencies of RB and SO, respectively. The data points are closely distributed along the 45-degree line, indicating excellent agreement between the predicted and actual values. Therefore, this observation confirms the validity and high predictive capability of the quadratic

TABLE 3 The CCD matrix.

Variables					%Removal of RB		%Removal of SO	
Run	NFO amount	pH	Pollutant concentration	Sonication time	Actual	Predicted	Actual	Predicted
1	0	0	0	0	85.10	84.89	89.69	90.41
2	1	−1	1	1	59.34	59.39	58.73	58.80
3	−2	0	0	0	44.38	43.97	48.88	49.01
4	2	0	0	0	77.61	77.43	77.18	76.80
5	1	−1	1	−1	41.56	42.00	45.36	45.89
6	−1	1	1	−1	37.77	38.08	53.10	54.09
7	−1	−1	1	−1	28.81	28.96	37.69	36.89
8	0	0	0	0	85.25	84.89	89.42	90.41
9	0	0	0	0	84.59	84.89	90.94	90.41
10	0	2	0	0	64.05	63.86	75.84	75.97
11	−1	−1	−1	1	59.70	59.98	63.30	63.48
12	0	0	0	−2	51.27	50.78	60.75	60.00
13	1	1	1	−1	57.60	57.53	67.19	66.86
14	−1	1	1	1	49.81	49.99	61.01	60.12
15	−1	1	−1	1	70.08	70.02	74.45	74.31
16	1	1	−1	1	90.37	90.44	92.45	93.10
17	−1	−1	−1	−1	54.78	55.06	56.26	56.90
18	1	−1	−1	1	73.92	73.99	79.09	78.50
19	−1	1	−1	−1	64.07	64.23	70.66	70.44
20	0	0	0	0	85.36	84.89	89.34	90.41
21	0	0	2	0	42.43	42.10	48.97	49.33
22	0	0	0	0	84.89	84.89	91.18	90.41
23	0	0	0	2	74.06	73.96	76.29	76.79
24	0	0	0	0	84.17	84.89	91.89	90.41
25	1	1	−1	−1	78.01	78.29	84.88	85.06
26	−1	−1	1	1	39.90	40.00	45.43	45.64
27	0	0	−2	0	83.11	82.85	85.98	85.38
28	1	−1	−1	−1	62.68	62.71	67.00	67.74
29	1	1	1	1	75.70	75.80	77.32	77.07
30	0	−2	0	0	38.69	38.29	44.54	44.17

models developed using CCD. Supplementary Figures S2c, d present the normal probability plots of the residuals for the removal of RB and SO, respectively. The residuals closely follow a straight line, demonstrating that the errors are normally distributed with constant variance and indicating the absence of significant systematic deviations in the developed models. This result further validates the adequacy and reliability of the models for predicting dye removal efficiencies under varying operational conditions. The combined evidence from ANOVA, statistical indices (R^2, Adjusted R^2, Predicted R^2, MSE, and RMSE), and graphical analyses confirms the robustness of the developed models and their applicability for process optimization in the ultrasound-assisted removal of RB and SO using NFO nanoparticles.

3.3 Response surface analysis

Three-dimensional response surface plots and contour plots were generated to evaluate the interactive effects of process variables

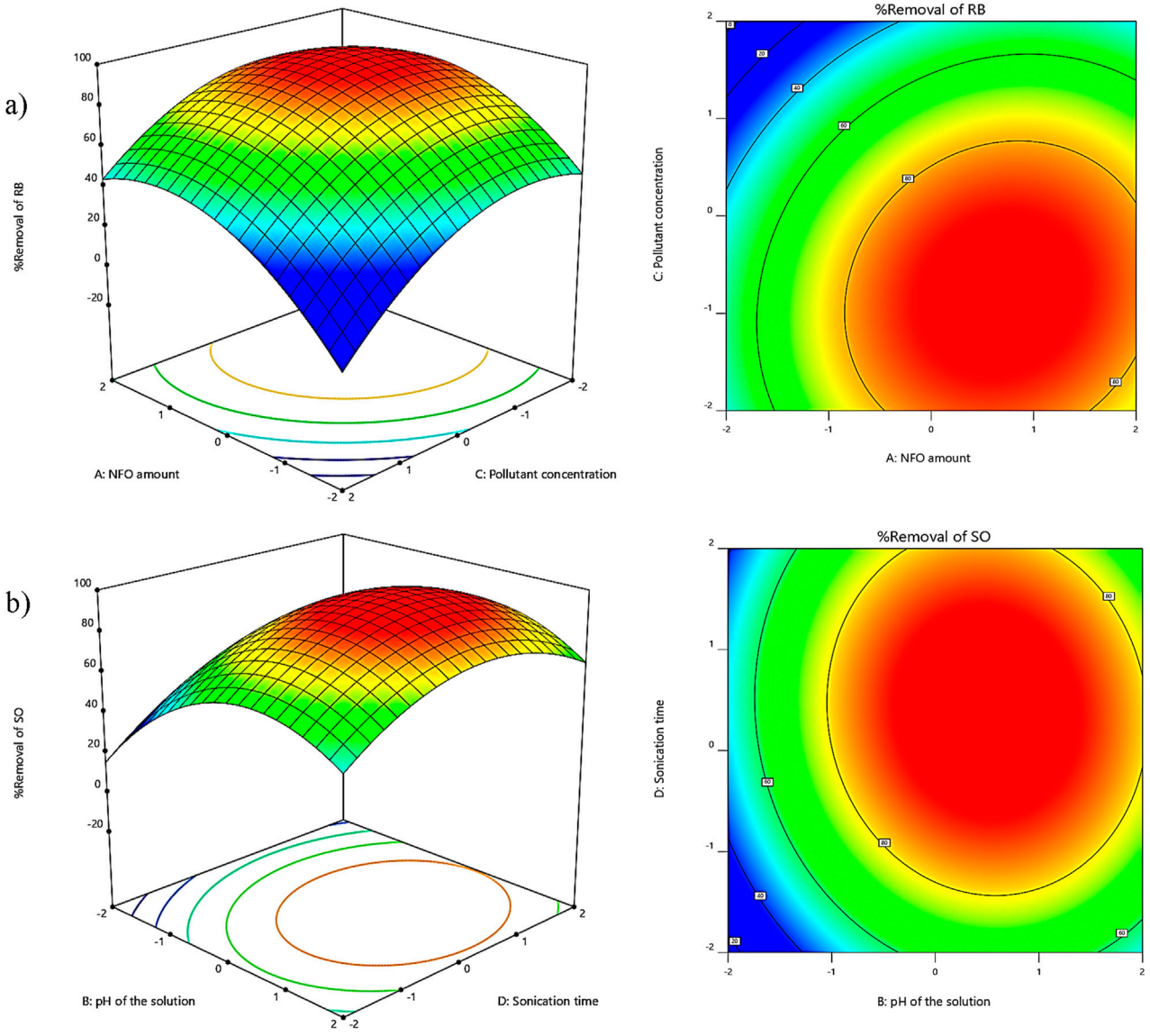

FIGURE 2
Response surface plots of removal of **(a)** RB and **(b)** SO.

on the removal efficiency of RB and SO using NFO nanoparticles under ultrasonic assistance. These plots provide a clear visualization of how the combination of two variables affects dye removal while keeping other variables constant at their central levels.

An increase in the NFO amount led to an enhancement in RB dye removal efficiency due to the increased availability of active sites for removal. However, at a constant adsorbent amount, increasing the initial dye concentration decreased the removal efficiency, likely due to the saturation of active sites on the adsorbent surface. For example, Figure 2a illustrates the interactive effect of NFO amount and dye concentration on the removal efficiency of RB at a fixed pH of 8 and a sonication time of 16 min, where the removal efficiency increases from 50% to 86% with increasing adsorbent amount at lower dye concentrations. Similar trends were reported by Joshi et al. in their study on dye removal using carbon-based adsorbents under an optimized amount (Joshi et al., 2022).

Analyzing the interactive effects of NFO amount and dye concentration demonstrated Figure 2a displays the combined influence of NFO amount and dye concentration on RB removal at a fixed pH of 8 and sonication time of 16 min, indicating that removal efficiency decreased from 88% to 47% as dye concentration increased from 15 to 45 mg L^{-1} at a constant NFO amount. Similar results were reported by Tamer et al. and Ma et al., confirming the consistency of these observations with previous studies (Tamer et al., 2024; Ma et al., 2022).

The effect of sonication time and solution pH was also investigated. Increasing the sonication time enhanced the dye removal efficiency due to improved dispersion of nanoparticles and enhanced mass transfer, up to a certain point where equilibrium was reached, and further increases in sonication time showed minimal effects. For instance, Figure 2b illustrates the combined effect of sonication time and pH on SO removal at an NFO amount of 0.038 g and a

TABLE 4 Optimal conditions for the removal process (N = 3).

Optimal conditions				%Removal ± %RSD			
				RB		SO	
A (g)	B	C (mg L^{-1})	D (min)	Actual	Predicted	Actual	Predicted
0.038	8	20	16	95.72 ± 2.1	93.64	97.33 ± 1.8	97.70

dye concentration of 20 mg L^{-1}, where the removal efficiency increased from 56% to 91% by increasing the sonication time. Saini et al. reported similar results in their study on the removal of crystal violet using bio-based adsorbents (Saini et al., 2025).

The solution pH plays a critical role in dye removal by influencing the surface charge of NFO nanoparticles and the ionization of dye molecules. Removal efficiency was found to increase under neutral to slightly alkaline conditions, favoring electrostatic interactions between the negatively charged surface of NFO (above its point of zero charge, pH_{pzc}) and the cationic dye molecules. In this respect, Figure 2b shows the interactive effects of pH and sonication time on RB removal at a fixed dye concentration of 20 mg L^{-1} and a NFO amount of 0.038 g. Here, removal efficiency increased significantly from 51% to 98% as the pH shifted from acidic to neutral and the sonication time increased. This observation is consistent with the findings reported by Younis et al. during pH optimization studies for dye removal (Younis et al., 2025).

These response surface analyses underscore the importance of optimizing operational parameters to maximize the removal efficiency of dyes using NFO nanoparticles under ultrasonic assistance, thereby supporting the findings obtained through statistical modeling and numerical optimization.

3.4 Optimization of operational parameters

Optimizing operational parameters is crucial for achieving maximum removal efficiency while ensuring the practical applicability of the process in real-world water treatment scenarios. In this study, numerical optimization was conducted using the desirability function within Design Expert software to determine the optimal conditions for the simultaneous removal of RB and SO using NFO nanoparticles under ultrasonic assistance. Based on the optimization analysis, the optimal conditions were identified as a solution pH of 8, a pollutant concentration of 20 mg L^{-1}, an NFO amount of 0.038 g, and a sonication time of 16 min (Table 4). Under these conditions, the predicted removal efficiencies were 93.64% for RB and 97.70% for SO, with an overall desirability value of 1, indicating that these conditions are suitable for achieving high removal efficiencies. Confirmatory experiments were conducted under the identified optimal conditions to validate the optimization results. In this regard, the removal efficiencies were found to be in close agreement with the predicted values, demonstrating 95.72% removal for RB and 97.33% for SO. The minor deviations observed can be attributed to experimental variability, confirming the accuracy and reliability of the developed models for process prediction and optimization. These findings demonstrate that integrating RSM with CCD provides an efficient and systematic approach for optimizing the ultrasound-assisted removal process using NFO nanoparticles.

TABLE 5 Desorption of pollutants from NFO nanoparticles (N = 3).

Eluents	%Removal ±% RSD	
	RB	SO
Toluene	54.69 ± 2.2	60.87 ± 2.5
Ethanol	91.43 ± 2.5	96.61 ± 2.3
Formic acid	37.64 ± 3.0	41.22 ± 1.9
Acetonitrile	72.15 ± 1.8	79.98 ± 2.8

3.5 Selection of eluent

Selecting an effective eluent is essential for the regeneration and reuse of NFO nanoparticles in dye removal processes. In this study, after completing the removal of RB and SO under optimal conditions, the NFO nanoparticles were separated using an external magnet and washed with deionized water to remove residual solution. Subsequently, the collected NFO nanoparticles were transferred into a tube containing 2 mL of different eluents (i.e., ethanol, acetonitrile, formic acid, and toluene) and stirred gently for 10 min at room temperature to facilitate desorption. After the elution process, the adsorbent was separated again using a magnet, and the supernatant was analyzed using a UV-Vis spectrophotometer to determine the concentration of desorbed dye. Among the tested eluents, ethanol exhibited the highest desorption efficiency for both RB (91.43%) and SO (96.61%), indicating its suitability for effective regeneration of NFO nanoparticles for reuse in repeated removal cycles (Table 5).

3.6 Regeneration and reusability of NFO nanoparticles

The regeneration and reuse of NFO nanoparticles are critical for reducing operational costs and ensuring the sustainability of the removal process. In this study, the reusability of NFO nanoparticles was evaluated over five consecutive adsorption-desorption cycles under optimal conditions (Figure 3). After

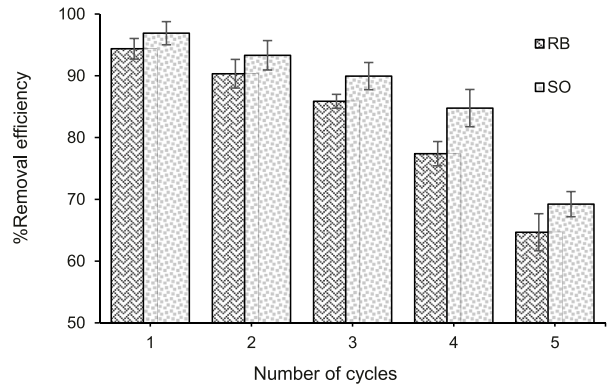

FIGURE 3
Efficiency of NFO nanoparticles for dyes removal in the cycles.

each adsorption cycle, the NFO nanoparticles were separated using an external magnet, washed with deionized water, and subjected to desorption using 2 mL of ethanol under gentle stirring for 10 min at room temperature. The adsorbent was then recollected magnetically, washed, and dried at 60 °C for 1 h before reuse in the next adsorption cycle. The removal efficiencies of RB and SO remained above 65% after five cycles, indicating minimal loss of adsorption capacity and confirming the stability and durability of NFO nanoparticles for repeated use in dye removal. The slight reduction in efficiency across cycles may be attributed to minor blockage of active sites or incomplete desorption, which is consistent with previous reports on the reusability of magnetic adsorbents (El Messaoudi et al., 2024). These findings highlight the potential of NFO nanoparticles as a stable, reusable adsorbent for practical applications in water treatment.

3.7 Interference studies

Interference studies under optimized conditions were conducted to evaluate the potential impact of co-existing ions on the removal performance of NFO nanoparticles. For this purpose, common ions including Na^{+}, Ni^{2+}, Zn^{2+}, F^{-}, and Hg^{2+} were selected as interfering species (Supplementary Table S3). In each experiment, a specific amount of NFO nanoparticles was added to 50 mL of dye solution containing the interfering ions under optimal pH, pollutant concentration, sonication time, and adsorbent amount. The mixture was subjected to ultrasonication for 16 min, followed by magnetic separation of the NFO nanoparticles. The supernatant was analyzed using a UV-Vis spectrophotometer to determine the residual dye concentration. The results indicated that the presence of these ions caused no significant interference, with removal efficiencies of RB and SO remaining above 95%. This result suggests that NFO nanoparticles possess high selectivity and stability for dye removal in the presence of common ions, confirming their potential applicability in real wastewater treatment.

3.8 Application to real samples

To evaluate the practical applicability of NFO nanoparticles for dye removal under real conditions, the optimized removal process was applied to various real water samples, including tap water, river water, and industrial wastewater collected from local sources. For this purpose, 50 mL of each water sample was spiked with known concentrations of RB and SO under optimal conditions (i.e., pH of 8, pollutant concentration of 20 mg L^{-1}, NFO amount of 0.038 g, and sonication time of 16 min). The mixture was subjected to ultrasonication, followed by magnetic separation of the adsorbent, and the supernatant was analyzed using a UV-Vis spectrophotometer to determine the remaining dye concentrations. The results demonstrated that the removal efficiencies in tap water, river water, and industrial

TABLE 6 Comparison of the NFO nanoparticles with different adsorbents for removal RB and SO.

Adsorbent	Analyte	Adsorbent amount	Time	pH	Concentration	Efficiency	Ref.
P-25 TiO_2 (Degussa)	RB	0.65 g	3 h	8	20 mg L^{-1}	80%	Soares et al. (2007)
Copper oxide nanoparticles	SO	1 g	24 h	6	50 mg L^{-1}	189 mg g^{-1}	Vidovix et al. (2022)
Waste seeds *Aleurites moluccana*	RB	0.05 g	1 h	6	30 mg L^{-1}	117 mg g^{-1}	Postai et al. (2016)
Ferric@nanocellulose/ nanohydroxyapatite	SO	2 g	24 h	7	300 mg L^{-1}	92.80%	Shaltout et al. (2024)
Modified orange peel (MOP)	RB	0.2 g	3 h	10	100 mg L^{-1}	85%	Oyekanmi et al. (2019)
Kaolinite (NRK) Clay	SO	2.5 g	15 min	7	100 mg L^{-1}	90%	Adebowale et al. (2014)
Activated carbon from argan nutshell	RB	0.01 g	1 h	5	33 mg L^{-1}	96.84%	Ouardi et al. (2024)
Silica mesoporous materials of MCM-48	SO	0.02 g	48 h	5	60 mg L^{-1}	62.5 mg g^{-1}	Abukhadra and Shaban (2019)
Moringa oliefera bark carbon	RB	0.025 g	1 h	6	30 mg L^{-1}	92%	Ramuthai et al. (2009)
Mesoporous graphite	SO	0.3 g	6 h	6	127 mg L^{-1}	100%	Shaban et al. (2018)
NFO nanoparticles	RB	0.038 g	16 min	8	20 mg L^{-1}	95.72%	Our work
NFO nanoparticles	SO	0.038 g	16 min	8	20 mg L^{-1}	97.33%	Our work

wastewater samples were consistent with those obtained in deionized water, achieving removal percentages of 96.83%, 92.89%, and 87.93% for RB and 97.79%, 94.03%, and 91.92% for SO, respectively (Supplementary Table S4). The minor decrease observed in wastewater samples may be attributed to the presence of organic and inorganic contaminants, which slightly compete for active sites on the NFO surface. These results confirm the efficiency and robustness of NFO nanoparticles for practical dye removal from various real water matrices under ultrasonic assistance.

3.9 Comparison with other adsorbents

To evaluate the performance of NFO nanoparticles more precisely, the obtained results were compared with previously reported adsorbents used for the removal of RB and SO from aqueous solutions (Table 6). The comparison considered parameters such as maximum removal efficiency, time, required adsorbent amount, and operational conditions. It was observed that while some adsorbents like activated carbon, agricultural wastes, and non-magnetic nanoparticles achieved high removal efficiencies, they often required higher amounts (up to 2.5 g), longer contact times (up to 48 h), and pH adjustments toward strongly acidic or alkaline conditions to maintain performance. In contrast, the NFO nanoparticles in this study achieved removal efficiencies above 95% for both dyes using a significantly lower amount (0.038 g), shorter contact time (16 min), and under near-neutral pH conditions. These findings suggest that NFO nanoparticles, when assisted by ultrasonic treatment, provide a competitive and efficient alternative for dye removal. The advantages of these nanoparticles include rapid separation using an external magnet, reusability over multiple cycles with minimal performance loss, and operational simplicity suitable for real water treatment applications.

4 Conclusion

In this study, NFO magnetic nanoparticles were successfully synthesized and applied for the ultrasound-assisted removal of RB and SO from aqueous solutions. The synthesized nanoparticles exhibited a nanometric size, high surface area, and superparamagnetic properties, enabling efficient dye removal and easy separation using an external magnet. Using RSM with CCD, the effects of pH, pollutant concentration, NFO amount, and sonication time on removal efficiency were systematically investigated and optimized. Under optimal conditions (i.e., pH of 8, pollutant concentration of 20 mg L^{-1}, NFO amount of 0.038 g, and sonication time of 16 min), removal efficiencies above 95% were achieved for RB and SO. The NFO nanoparticles demonstrated excellent reusability over multiple adsorption-desorption cycles using ethanol as an eluent, maintaining removal efficiencies above 65%. The removal efficiency of RB and SO was obtained in the range of 87.93%–97.79% for the real samples. Interference studies confirmed the high selectivity of the nanoparticles in the presence of co-existing ions, and application to real water samples validated their efficiency in practical conditions. Overall, the results indicate that NFO nanoparticles, under ultrasonic assistance, represent a promising, reusable, and efficient adsorbent for the rapid removal of dyes from water, supporting their potential application in sustainable wastewater treatment systems.

Data availability statement

The original contributions presented in the study are included in the article/Supplementary Material, further inquiries can be directed to the corresponding author.

Author contributions

IA: Methodology, Writing – review and editing. DA: Writing – review and editing, Formal analysis. VJ: Project administration, Writing – review and editing. AK: Formal analysis, Writing – review and editing. MR: Writing – review and editing, Data curation. MK: Writing – review and editing, Data curation. SSu: Writing – review and editing, Writing – original draft. SR: Data curation, Writing – review and editing. SSh: Writing – original draft, Writing – review and editing.

Funding

The author(s) declare that financial support was received for the research and/or publication of this article. The authors are thankful to the Deanship of Scientific Research, King Khalid University, Abha, Saudi Arabia, for financially supporting this work through the Large Research Group Project under Grant no. R.G.P.2/410/46.

Conflict of interest

The authors declare that the research was conducted in the absence of any commercial or financial relationships that could be construed as a potential conflict of interest.

Generative AI statement

The author(s) declare that no Generative AI was used in the creation of this manuscript.

Publisher's note

Supplementary material

The Supplementary Material for this article can be found online at: https://www.frontiersin.org/articles/10.3389/fenvs.2025.1622134/full#supplementary-material

References

Abukhadra, M. R., and Shaban, M. (2019). Recycling of different solid wastes in synthesis of high-order mesoporous silica as adsorbent for safranin dye. *Int. J. Environ. Sci. Technol.* 16 (11), 7573–7582. doi:10.1007/s13762-019-02231-8

Adebowale, K. O., Olu-Owolabi, B. I., and Chigbundu, E. C. (2014). Removal of safranin-O from aqueous solution by adsorption onto kaolinite clay. *J. Encapsulation Adsorpt. Sci.* 4 (03), 89–104. doi:10.4236/jeas.2014.43010

Al-Saeedi, S. I., Areej, A., Qamar, M. T., Alhujaily, A., Iqbal, S., Alotaibi, M. T., et al. (2023). Isotherm and kinetic studies for the adsorption of methylene blue onto a novel Mn3O4-Bi2O3 composite and their antifungal performance. *Front. Environ. Sci.* 11, 1156475. doi:10.3389/fenvs.2023.1156475

Alharbi, H. A., Hameed, B. H., Alotaibi, K. D., Al-Oud, S. S., and Al-Modaihsh, A. S. (2022). Recent methods in the production of activated carbon from date palm residues for the adsorption of textile dyes: a review. *Front. Environ. Sci.* 10, 996953. doi:10.3389/fenvs.2022.996953

Ali, R., Mahmood, T., Naeem, A., Ullah, A., Aslam, M., and Khan, S. (2021). Process optimization of auramine O adsorption by surfactant-modified activated carbon using box–behnken design of response surface methodology. *Desalin. Water Treat.* 217, 367–390. doi:10.5004/dwt.2021.26740

Aragaw, T. A., and Bogale, F. M. (2021). Biomass-based adsorbents for removal of dyes from wastewater: a review. *Front. Environ. Sci.* 9, 764958. doi:10.3389/fenvs.2021.764958

Bayuo, J., Rwiza, M. J., Choi, J. W., Mtei, K. M., Hosseini-Bandegharaei, A., and Sillanpää, M. (2024). Adsorption and desorption processes of toxic heavy metals, regeneration and reusability of spent adsorbents: economic and environmental sustainability approach. *Adv. Colloid Interface Sci.* 329, 103196. doi:10.1016/j.cis.2024.103196

Bopape, D. A., Ntsendwana, B., and Mabasa, F. D. (2024). Photocatalysis as a pre-discharge treatment to improve the effect of textile dyes on human health: a critical review. *Heliyon* 10, e39316. doi:10.1016/j.heliyon.2024.e39316

Çalışkan, B., and Şayan, E. (2024). A brief overview of the effects of ultrasound on the adsorption/desorption process: a review. *Int. J. Environ. Anal. Chem.* 104 (16), 3821–3851. doi:10.1080/03067319.2022.2093641

El Messaoudi, N., El Khomri, M., El Mouden, A., Bouich, A., Jada, A., Lacherai, A., et al. (2024). Regeneration and reusability of non-conventional low-cost adsorbents to remove dyes from wastewaters in multiple consecutive adsorption–desorption cycles: a review. *Biomass Convers. biorefin.* 14 (11), 11739–11756. doi:10.1007/s13399-022-03604-9

Garg, B., Sethi, P., and Basu, S. (2025). Strategic innovation in CuBTC/PANI nanocomposites for dye remediation: a holistic approach for enhancing adsorption, isotherms, and kinetic studies. *RSC Sustain.* 3 (5), 2311–2324. doi:10.1039/d5su00056d

Hariharasuthan, R., Chitradevi, S., Radha, K. S., and Chithambaram, V. (2022). Characterization of NiFe2O4 (nickel ferrite) nanoparticles with very low magnetic saturation synthesized *via* co-precipitation method. *Appl. Phys. A* 128 (12), 1045. doi:10.1007/s00339-022-06163-y

Hassan, A. A., Ali, M. E. M., Abdel-Latif, S. A., Hasani, I. W., and Fahim, Y. A. (2025). Efficient removal of remazol red dye from aqueous solution using magnetic nickel ferrite nanoparticles synthesized *via* aqueous reflux. *Sci. Rep.* 15 (1), 17527–17. doi:10.1038/s41598-025-98478-y

He, X., Chen, X., Wang, X., and Jiang, L. (2023). Optimization of activated carbon production from corn cob using response surface methodology. *Front. Environ. Sci.* 11, 1105408. doi:10.3389/fenvs.2023.1105408

Hoong, H. N. J., and Ismail, N. (2018). Removal of dye in wastewater by adsorption-coagulation combined system with Hibiscus sabdariffa as the coagulant." In MATEC web of conferences, EDP Sciences, 152, 01008.

Hsu, C. Y., Ali, E., Al-Saedi, H. F. S., Mohammed, A. Q., Mustafa, N. K., Talib, M. B., et al. (2024). A chemometric approach based on response surface methodology for optimization of antibiotic and organic dyes removal from water samples. *BMC Chem.* 18 (1), 5. doi:10.1186/s13065-023-01107-w

Iqbal, Z., Tanweer, M. S., and Alam, M. (2022). Recent advances in adsorptive removal of wastewater pollutants by chemically modified metal oxides: a review. *J. Water Process Eng.* 46, 102641. doi:10.1016/j.jwpe.2022.102641

Jassim, N. J., Younis, F. H., and Alshamkhani, M. T. (2025). Adsorption of safranin-O dye onto almond shell sustainable activated carbon: identifying key process factors and their effects. *Eng. Rep.* 7 (1), e13121. doi:10.1002/eng2.13121

Joshi, P., Prolta, A., Mehta, S., Khan, T. S., Srivastava, M., and Khatri, O. P. (2022). Adsorptive removal of multiple organic dyes from wastewater using regenerative microporous carbon: decisive role of surface-active sites, charge and size of dye molecules. *Chemosphere* 308, 136433. doi:10.1016/j.chemosphere.2022.136433

Kalsoom, K., Ali, A., Khan, S., Ali, N., and Khan, M. A. (2024). Enhanced ultrasonic adsorption of pesticides onto the optimized surface area of activated carbon and biochar: adsorption isotherm, kinetics, and thermodynamics. *Biomass Convers. biorefin.* 14 (14), 15519–15534. doi:10.1007/s13399-023-04170-4

Khandelwal, D., Rana, I., Mishra, V., Ranjan, K. R., and Singh, P. (2024). Unveiling the impact of dyes on aquatic ecosystems through Zebrafish–A comprehensive review. *Environ. Res.* 261, 119684. doi:10.1016/j.envres.2024.119684

Li, B., Qi, B., Guo, Z., Wang, D., and Jiao, T. (2023). Recent developments in the application of membrane separation technology and its challenges in oil-water separation: a review. *Chemosphere* 327, 138528. doi:10.1016/j.chemosphere.2023.138528

Liu, P., Lyu, J., and Bai, P. (2025). Synthesis of mixed matrix membrane utilizing robust defective MOF for size-selective adsorption of dyes. *Sep. Purif. Technol.* 354, 128672. doi:10.1016/j.seppur.2024.128672

Ma, X., Zhao, S., Tian, Z., Duan, G., Pan, H., Yue, Y., et al. (2022). MOFs meet wood: reusable magnetic hydrophilic composites toward efficient water treatment with super-high dye adsorption capacity at high dye concentration. *Chem. Eng. J.* 446, 136851. doi:10.1016/j.cej.2022.136851

Ouardi, Y. E., Aissouq, A. E., Chennah, A., Ouammou, A., and Laatikainen, K. (2024). Synthesis, characterization, and DFT investigation of rhodamine B dye removal by activated carbon produced from argan nutshell. *Biomass Convers. biorefin.* 14 (13), 15107–15118. doi:10.1007/s13399-022-03706-4

Oyekanmi, A. A., Ahmad, A., Hossain, K., and Rafatullah, M. (2019). Statistical optimization for adsorption of Rhodamine B dye from aqueous solutions. *J. Mol. Liq.* 281, 48–58. doi:10.1016/j.molliq.2019.02.057

Oza, S., Kodgire, P., and Kachhwaha, S. S. (2022). Analysis of RSM based BBD and CCD techniques applied for biodiesel production from waste cotton-seed cooking oil *via* ultrasound method. *Anal. Chem. Lett.* 12 (1), 86–101. doi:10.1080/22297928.2021.2019611

Peramune, D., Manatunga, D. C., Dassanayake, R. S., Premalal, V., Liyanage, R. N., Gunathilake, C., et al. (2022). Recent advances in biopolymer-based advanced oxidation processes for dye removal applications: a review. *Environ. Res.* 215, 114242. doi:10.1016/j.envres.2022.114242

Postai, D. L., Demarchi, C. A., Zanatta, F., Melo, D. C. C., and Rodrigues, C. A. (2016). Adsorption of rhodamine B and methylene blue dyes using waste of seeds of Aleurites moluccana, a low cost adsorbent. *Alex. Eng. J.* 55 (2), 1713–1723. doi:10.1016/j.aej.2016.03.017

Prabhu, S. M., Rane, N. R., Li, X., Otari, S. V., Girawale, S. D., Palake, A. R., et al. (2023). Magnetic nanostructured adsorbents for water treatment: structure-Property relationships, chemistry of interactions, and lab-to-industry integration. *Chem. Eng. J.* 468, 143474. doi:10.1016/j.cej.2023.143474

Preethi, S., Sivasamy, A., Sivanesan, S., Ramamurthi, V., and Swaminathan, G. (2006). Removal of safranin basic dye from aqueous solutions by adsorption onto corncob activated carbon. *Ind. Eng. Chem. Res.* 45 (22), 7627–7632. doi:10.1021/ie0604122

Ramuthai, S., Nandhakumar, V., Thiruchelvi, M., Arivoli, S., and Vijayakumaran, V. (2009). Rhodamine B adsorption-kinetic, mechanistic and thermodynamic studies. *J. Chem.* 6, S363–S373. doi:10.1155/2009/470704

Saini, P., Chakinala, N., Surolia, P. K., and Chakinala, A. G. (2025). Ultrasound-assisted enhanced adsorption of textile dyes with metal organic frameworks. *Sep. Purif. Technol.* 354, 128730. doi:10.1016/j.seppur.2024.128730

Samad, S. A., Arafat, A., Lester, E., and Ahmed, I. (2022). Upcycling glass waste into porous microspheres for wastewater treatment applications: efficacy of dye removal. *Materials* 15 (17), 5809. doi:10.3390/ma15175809

Sarkar, S., Chakraborty, P., and Das, P. (2025). Synthesis of nano-silica-coated peanut shell-derived bio-char composite for removal of safranin dye present in aqueous solution: batch and optimization using response surface methodology. *Biomass Convers. biorefin.* 15 (1), 1139–1154. doi:10.1007/s13399-024-05389-5

Shaban, M., Abukhadra, M. R., Mohamed, A. S., Shahien, M. G., and Ibrahim, S. S. (2018). Synthesis of mesoporous graphite functionalized by nitrogen for efficient removal of safranin dye utilizing rice husk ash; equilibrium studies and response surface optimization. *J. Inorg. Organomet. Polym. Mater.* 28, 279–294. doi:10.1007/s10904-017-0726-2

Shaltout, W. A., El-Naggar, G. A., Esmail, G., and Hassan, A. F. (2024). Synthesis and characterization of ferric@ nanocellulose/nanohydroxyapatite bio-composite based on sea scallop shells and cotton stalks: adsorption of Safranin-O dye. *Biomass Convers. biorefin.* 14 (4), 4759–4776. doi:10.1007/s13399-022-02753-1

Shojaei, S., Shojaei, S., Nouri, A., and Baharinikoo, L. (2021). Application of chemometrics for modeling and optimization of ultrasound-assisted dispersive liquid–liquid microextraction for the simultaneous determination of dyes. *NPJ Clean. Water* 4 (1), 23. doi:10.1038/s41545-021-00113-6

Singh, N., Malik, A., Nohwar, S., Jana, R., and Mondal, P. C. (2023). Covalent surface modification of nickel ferrite nanoparticles for electrochemical supercapacitor performance. *New J. Chem.* 47 (11), 5308–5315. doi:10.1039/d2nj05566j

Sivakumar, P., Ramesh, R., Ramanand, A., Ponnusamy, S., and Muthamizhchelvan, C. (2013). Synthesis and characterization of NiFe2O4 nanoparticles and nanorods. *J. Alloys Compd.* 563, 6–11. doi:10.1016/j.jallcom.2013.02.077

Soares, E. T., Lansarin, M. A., and Moro, C. C. (2007). A study of process variables for the photocatalytic degradation of rhodamine B. *Braz. J. Chem. Eng.* 24, 29–36. doi:10.1590/s0104-66322007000100003

Tamer, T. M., Abbas, R., Sadik, W. A., Omer, A. M., Abd-Ellatif, M. M., and Mohy-Eldin, M. S. (2024). Development of novel amino-ethyl chitosan hydrogel for the removal of methyl Orange azo dye model. *Sci. Rep.* 14 (1), 1284. doi:10.1038/s41598-024-51538-1

Teweldebrihan, M. D., Gnaro, M. A., and Dinka, M. O. (2024). The application of magnetite biochar composite derived from Parthenium hysterophorus for the adsorption of methylene blue from aqueous solution. *Front. Environ. Sci.* 12, 1375437. doi:10.3389/fenvs.2024.1375437

Tkaczyk, A., Mitrowska, K., and Posyniak, A. (2020). Synthetic organic dyes as contaminants of the aquatic environment and their implications for ecosystems: a review. *Sci. Total Environ.* 717, 137222. doi:10.1016/j.scitotenv.2020.137222

Ugural, M. N., Aghili, S., and Burgan, H. I. (2024). Adoption of lean construction and AI/IoT technologies in iran's public construction sector: a mixed-methods approach using fuzzy logic. *Buildings* 14 (10), 3317. doi:10.3390/buildings14103317

Vidovix, T. B., Quesada, H. B., Bergamasco, R., Vieira, M. F., and Vieira, A. M. S. (2022). Adsorption of Safranin-O dye by copper oxide nanoparticles synthesized from Punica granatum leaf extract. *Environ. Technol.* 43 (20), 3047–3063. doi:10.1080/09593330.2021.1914180

Yang, J., Shojaei, S., and Shojaei, S. (2022). Removal of drug and dye from aqueous solutions by graphene oxide: adsorption studies and chemometrics methods. *NPJ Clean. Water* 5 (1), 5. doi:10.1038/s41545-022-00148-3

Younis, S. R., Abdelmotallieb, M., and Ahmed, A. S. (2025). Facile synthesis of ZIF-8@ GO composites for enhanced adsorption of cationic and anionic dyes from their aqueous solutions. *RSC Adv.* 15 (11), 8594–8608. doi:10.1039/d4ra08890e